Enhanced photoactivity on Ag/Ag₃PO₄ composites by plasmonic effect

Mohammed Ashraf Gondal [a,*], Xiaofeng Chang [a,b], Wei E.I. Sha [c], Zain Hassan Yamani [a], Qin Zhou [d]

[a] Laser Research Group, Physics Department and Center of Excellence in Nanotechnology, King Fahd University of Petroleum and Minerals, Dhahran 31261, Saudi Arabia
[b] College of Materials Science and Technology, Nanjing University of Aeronautics and Astronautics, Nanjing 211100, China
[c] Department of Electrical and Electronic Engineering, University of Hong Kong, Pokfulam Road, Hong Kong
[d] State Key Laboratory of Environmental Aquatic Chemistry, Research Center for Eco-Environmental Sciences, Chinese Academy of Sciences, Beijing 100085, China

ARTICLE INFO

ABSTRACT

The work presented here deals with the photoreduction in metallic silver nanoparticles onto the surface of Ag₃PO₄ and resulting photocatalytic activity enhancement toward degradation of dye molecules, namely Rhodamine B (Rh. B) as a model compound, from aqueous solution under UV or visible light irradiation. Our results clearly indicated that the photoactivity of Ag₃PO₄ was significantly enhanced by depositing an optimum amount of silver nanoparticles, even though the adsorption kinetics rate and capacity decreased after the silver nanoparticles agglomerate extensively. The surface plasmon resonance (SPR) excited between the silver nanoparticles and Rh. B interface is a physical origin and responsible for the boosted photoactivity, which strongly depends on the specific wavelength of the incident light. This work provides and suggests a novel scheme for Ag/Ag₃PO₄ composites having plasmonic effect on the interface with detailed experimental and theoretical study.

1. Introduction

Heterogeneous photocatalysis technology has become a promising approach to solve energy and environmental problems since 1972 [1]. The concept of "low-carbon & green life" as well as the pioneer achievements by scholars such as Asahi et al. [2], Zou et al. [3] are inspiring and great enthusiasm to develop highly efficient photocatalysts to improve the quantum efficiency under visible light (380–780 nm), which represents around 42 % of the total light spectrum of the solar radiations [4,5].

In early 2010, silver orthophosphate (Ag₃PO₄) was reported as an active semiconductor, which showed an extremely high photocatalytic performance with quantum efficiency over 90% at wavelengths longer than 420 nm [6]. Soon after, synthesis of single-crystalline Ag₃PO₄ sub-microcrystals with selective facets [7], colloidal Ag₃PO₄ nanocrystals [8], Ag₃PO₄ sub-microcrystals [9,10], Ag₃PO₄ nanowires [11], and AgX/Ag₃PO₄ (X = Cl, Br, I) [12] composites were reported. It has been widely documented and experimentally confirmed that the Ag₃PO₄ could be partially reduced to metallic Ag under visible light illumination, which undesirably leads to the catalyst leaching. However, a recent work by Huang et al. demonstrated that a combination of metallic silver with a series of silver salts based photocatalysts can improve their photocatalytic activity to different extents, depending on the types

of negatively charged ions (e.g., Cl⁻, Br⁻, I⁻, CrO₄²⁻, PO₄³⁻, PW₁₂O₄₀³⁻ and SiW₁₂O₄₀⁴⁻) in the corresponding semiconductor crystals [13]. The photocatalytic activity enhancement was attributed to localized surface plasmon resonance (LSPR) induced by metallic silver nanoparticles deposited on the surfaces of the silver salt photocatalysts.

Generally, surface plasmon resonance (SPR) for planar surfaces or localized surface plasmon resonance (LSPR) for nanoscaled metal particles can be induced by the excitation of surface plasmons (also known as surface plasmon polaritons, SPP) by using proper wavelength photons. The unique properties of surface plasmon have found a number of promising applications, such as heterogeneous photocatalysis [14,15], sensors [16], and photovoltaic cell [17,18].

Although the plasmonic effect of metallic nanoparticles on photocatalysis has been reported recently using wide spectrum of visible light for various photocatalysts, the report on monochromatic responses of these materials in terms of photocatalytic enhancement is very rare. As it is known, the extent of SPR and LSPR is highly dependent on the wavelengths of incident photons, so investigation into monochromatic response of these materials deserves much more attentions than it currently receives.

In this investigation, a series of Ag/Ag₃PO₄ composites were prepared by a facile photochemical method, and their monochromatic response (i.e., 350, 420, 450, 500 nm) was investigated by photodegradation of a model compound (i.e., Rhodamine B (Rh. B)). Rh. B photodegradation in water was found to be strongly

* Corresponding author. Fax: +966 38602293.
E-mail address: magondal@kfupm.edu.sa (M.A. Gondal).

dependent on the wavelength of incident light and the amount of surface silver nanoparticles on Ag_3PO_4, which is substantiated well by physics simulation results.

2. Experimental and calculation method

2.1. Experimental method

2.1.1. Preparation of Ag/Ag$_3$PO$_4$ composites

All the chemicals used in this study were of analytical grade and used as received without further purification. Absolute ethanol (C_2H_5OH), silver nitrate ($AgNO_3$), disodium hydrogen phosphate (Na_2HPO_4), and Rhodamine B (Rh. B) were purchased from Sigma-Aldrich. Ultrapure Milli-Q water obtained by Millipore was used for the preparation of solutions.

Semiconductor compound of Ag_3PO_4 was prepared as per procedure described in the literature [6] by using $AgNO_3$ and Na_2HPO_4 as the starting materials. The obtained Ag_3PO_4 powders of 2 g dispersed in water of 200 mL were then irradiated under full-arc light emitted from Xenon lamp having power of 300 Watts (Beijing Trusttech Co. Ltd., PLS-SXE-300) for different time of 1, 2, 5, and 10 h. The final products were obtained after separation from water by centrifugation at 10,000 rpm, washing with absolute ethanol/water several times and drying at 60 °C. The as-prepared series composites were named according to the preparation conditions as illustrated by "Ag/Ag$_3$PO$_4$-x," where "x" denotes the irradiation time (hour) for the preparation.

2.1.2. Characterization

The crystal structures of the Ag/Ag$_3$PO$_4$ composites before and after photochemical reaction were determined by X-ray diffractometer (XRD, Bruker D8 ADVANCE) with 2θ scope of 10–90° using Cu Kα X-ray source (λ = 0.15418 nm). X-ray photoelectron spectroscopy (XPS) study was carried out by multi-technique surface analyzer (Kratos AXIS Ultra DLD). Scanning transmission electron microscope (STEM) images of samples were taken on a transmission electron microscope (Tecnai T12) and field emission gun-scanning electron microscope (Quanta 600 FEG), respectively.

2.1.3. Adsorption and photocatalytic performance

Batch experiments were performed in order to investigate the effect of combination of silver nanoparticles with Ag_3PO_4 on sorption capacity toward probe molecules (Rh. B). Aqueous solution of Rhodamine dye with desired concentration was prepared, required amount of Ag/Ag$_3$PO$_4$ composite was added, and the resulting suspension was shaken in an orbital shaker (150 rpm) at room temperature. After experiments, the catalyst was separated by centrifugation at 10,000 rpm, and the absorbance of Rh. B was determined by UV–vis spectrophotometer (UV-2550, Shimadzu) following the absorption maxima (λ_{max}) of dye, which was found to be at 554 nm.

The adsorption kinetics is one of the most significant tools to describe the adsorption behavior of any compound. In this study, the pseudo-1st-order adsorption kinetic model was adopted to evaluate and calculate the solute uptake rate and the corresponding thermal dynamical parameters. The pseudo-1st-order adsorption kinetic equation can be written as follows [19],

$$q_t = q_e(1 - e^{-k_1 t/2.303}) \tag{1}$$

where q_t (μmol g^{-1}) is the adsorption capacity at specific contact time, k_1 (min^{-1}) is the pseudo-1st-order kinetic constant, and t is the adsorption time.

Adsorption isotherm is another significant approach to evaluate the adsorption capacity of adsorbents as well as to understand the interactions between adsorbate and adsorbent. To investigate the isothermal behavior of Rh. B adsorption, typical isothermal models, that is, Langmuir and Freundlich, were adopted.

For Langmuir model, the adsorption can be expressed as follows [20]:

$$q_e = \frac{q_m K_L C_e}{1 + K_L C_e} \tag{2}$$

where q_e is the adsorption amount at equilibrium (μmol g^{-1}), C_e is the equilibrium concentration of the aqueous solution (μmol L^{-1}), q_m is the maximum adsorption capacity (μmol g^{-1}), and K_L is the constant related to the free energy of adsorption (L mg^{-1}).

The Freundlich model for adsorption of Rh. B can be written as follows [21]:

$$q_e = K_F C_e^{1/n} \tag{3}$$

where K_F (μmol$^{1-(1/n)}$ L$^{1/n}$ g^{-1}) and n are two constants, indicating the relative adsorption capacity and the intensity of the adsorption, respectively. The symbols q_e and C_e represent the adsorption amount at equilibrium (μmol g^{-1}) and equilibrium concentration of the aqueous solution (μmol L^{-1}), respectively.

A 300 W Xenon lamp (Beijing Trusttech Co. Ltd., PLS-SXE-300) was selected as the light source. Series of band-pass filters (350 nm, 420 nm, 450 nm, 500 nm, and 550 nm) were used to obtain different wavelengths as incident monochromatic light. After photochemical reactions, the catalyst was removed by centrifugation (14,000 rpm), and the absorbance of the resulting dye solution was determined.

2.2. Calculation method for scattering cross section [22–24]

The scattering cross section, which can estimate the scattering strength of a metallic nanostructure, is defined by

$$\sigma_s = \frac{\int_s \text{Re}\left[\frac{1}{2}E^S \times conj(H^S)\right] \cdot dS}{|S_i|} \tag{4}$$

where "conj" denotes the complex conjugation, S is an arbitrary surface enclosing the metallic nanostructure, $S_i = \frac{1}{2}[E^i \times conj(H^i)]$ is the incident energy flux, and E^s and H^s are the scattered electric and magnetic fields, respectively.

The scattering cross section of a nanosphere can be obtained from Mie series or the generalized reflection coefficient of the spherically layered media

$$\sigma_s = \frac{2\pi}{K_2^2} \sum_{m=1}^{\infty} (2m+1)\left(\left|\widetilde{R}_{2,1}^{TM}(m)\right|^2 + \left|\widetilde{R}_{2,1}^{TE}(m)\right|^2\right) \tag{5}$$

where 1 and 2 denote the metallic (silver) and the dielectric (Rhodamine B aqueous solution) background layer, respectively, m is the order of the modified spherical Bessel (Hankel) functions, and $\widetilde{R}_{2,1}^{TM}$ and $\widetilde{R}_{2,1}^{TE}$ are the generalized reflection coefficients of the TM and TE spherical waves in the layer 2 reflected by the layer 1. For small spherical particles, the leading term ($m = 1$) of $\widetilde{R}_{2,1}^{TM}$ determines the value of the scattering cross section, which is given by

$$R_{i,i-1}^{TM} = \frac{\sqrt{\varepsilon_i \mu_{i-1}}\hat{j}_m(K_i r_{i-1})\hat{j}'_m(K_{i-1} r_{i-1}) - \sqrt{\varepsilon_{i-1} \mu_i}\hat{j}'_m(K_i r_{i-1})\hat{j}_m(K_{i-1} r_{i-1})}{\sqrt{\varepsilon_{i-1} \mu_i}\hat{j}_m(K_{i-1} r_{i-1})\hat{H}_m^{(1)'}(K_i r_{i-1}) - \sqrt{\varepsilon_i \mu_{i-1}}\hat{H}_m^{(1)'}(K_i r_{i-1})\hat{j}'_m(K_{i-1} r_{i-1})} \tag{6}$$

where r_i, ε_i, and K_i are the radius, permittivity, permeability, and wave number of the i th spherical layer, respectively. The scattering cross section can be normalized to the geometrical cross section of the nanosphere.
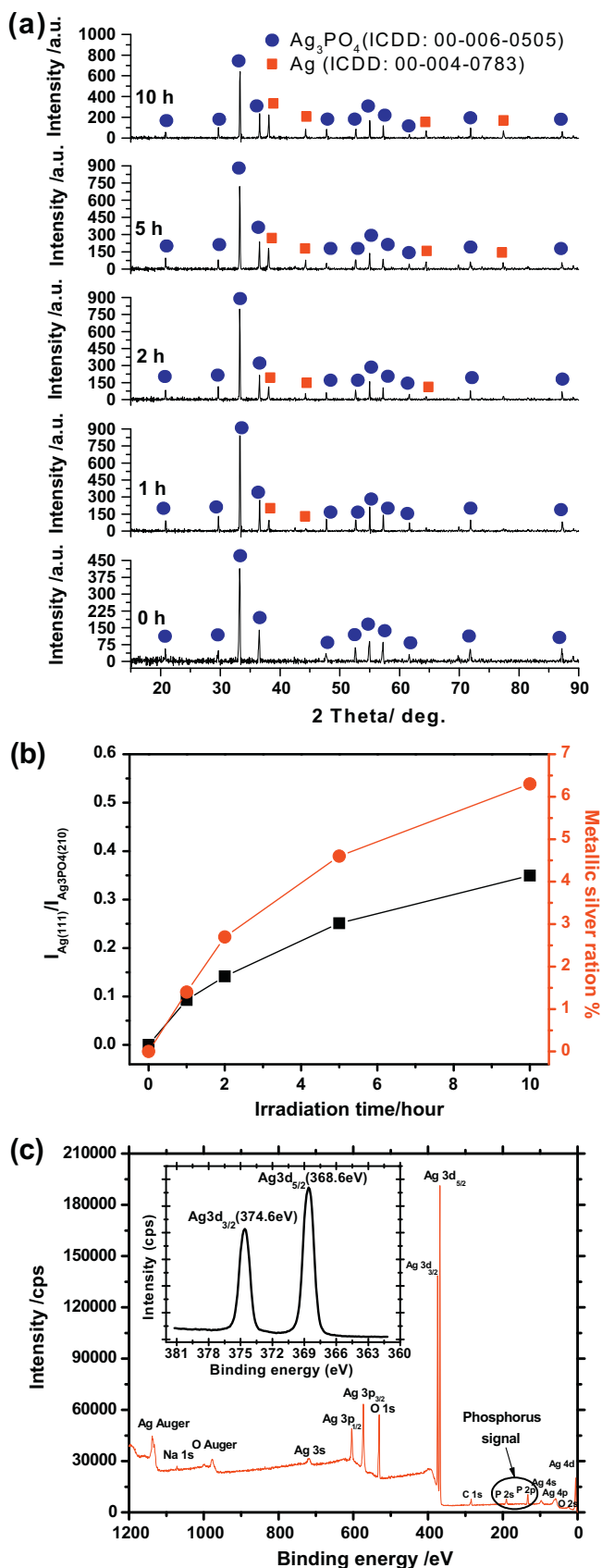
Fig. 1. XRD patterns of Ag/Ag$_3$PO$_4$ samples prepared under visible light irradiation for 0 h (i.e., pure phase of Ag$_3$PO$_4$), 1, 2, 5, and 10 h (a); changes of diffraction intensity ratios of Ag(111)/Ag$_3$PO$_4$(210) and metallic silver ratios as a function of photochemical reaction time (secondary axis has an error: 'ration' is a mistake of "ratio"), as well as low-resolution XPS of Ag/Ag$_3$PO$_4$ prepared by irradiating Ag$_3$PO$_4$ powder for 2 h (inset Fig. depicts the high-resolution XPS).

3. Results and discussion

Fig. 1a depicts XRD patterns of the Ag/Ag$_3$PO$_4$ composites synthesized under different irradiation time. Clearly, after certain time duration of visible light irradiation, the characteristic XRD patterns of the Ag$_3$PO$_4$ remained more or less unaffected. However, some new peaks, such as at 38.1°, 44.2°, 64.5°, and 77.4°, emerged, which can be ascribed to the silver crystal indexes of (111), (200), (220) and (311), respectively. This confirms the formation of Ag on the surfaces of Ag$_3$PO$_4$. Fig. 1b depicts the changes of the strongest diffraction intensity ratio ($I_{Ag(111)}/I_{Ag3PO4(210)}$) with the irradiation time. A nonlinear increase of $I_{Ag(111)}/I_{Ag3PO4(210)}$ ratios with irradiation time implies that the phase ratios of Ag/Ag$_3$PO$_4$ were gradually headed to a saturation regime with a prolonged irradiation time. A possible explanation might be that the in situ formed silver nanoparticles deposited on and covered the surface of Ag$_3$PO$_4$, which in turn inhibits the photochemical reduction of Ag$_3$PO$_4$ to Ag^0 because the surface silver nanoparticles could isolate photogenerated holes from water molecules and could block the visible light absorption of Ag$_3$PO$_4$ to a certain extent. The amount of metallic silver was formed that was estimated to be around 1.4%, 2.7%, 4.6%, and 6.3% (wt.%) of the samples under the irradiation for 1, 2, 5, and 10 h (Fig. 1b).

XPS results indicate that as-prepared samples were composed of silver, oxygen, and phosphorus (Fig. 1c). The existence of phosphorus and oxygen signals in the XPS pattern reveals that metallic silver nanoparticles could not completely cover the surface of Ag$_3$PO$_4$. The spin–orbit peaks centered at 374.6 eV and 368.6 eV (inset figure), which were corrected with a reference to C 1s (284.6 eV), correspond to the binding energy of Ag$d_{3/2}$ and Ag$d_{5/2}$, respectively, confirming the formation of metallic silver surface on the surface of Ag$_3$PO$_4$.

The formed silver nanoparticles can be clearly observed from SEM images of as-prepared samples (see the Supporting Information, Fig. S1). Based on the characterization results above, we could assume the average diameters of metallic silver and Ag$_3$PO$_4$ are 0.05 μm and 1 μm, respectively. Therefore, the mass of each Ag$_3$PO$_4$ particle can be obtained at 3.31×10^{-12} g ($\rho(Ag_3PO_4) = 6.37$ g cm^{-3}). If a thin film of silver (with thickness of 50 nm) covers one Ag$_3$PO$_4$ particle completely (i.e., monolayer coverage), the needed mass of metallic silver is at least 1.82×10^{-12} g ($\rho(Ag) = 10.5$ g cm^{-3}), that is, the coverage ratio of metallic silver should be $\geqslant 55.0$ wt.%. Our semi-quantification results suggest that the metallic silver ratios for all the samples are less than 10%, which are far lower than the theoretical value. Therefore, it can be deduced that the surface of Ag$_3$PO$_4$ cannot be completely covered by photoreduced metallic silver nanoparticles in this study. These theoretical results are well in agreement with the experimental results of SEM and XPS.

Low-resolution STEM characterization shows that some black points could form after irradiation by electron beam, which clearly shows the low stability of Ag$_3$PO$_4$ under electron irradiation and the reduction of Ag (bonded) by electron beam irradiation. Unfortunately, we were failed to obtain the STEM images of the as-prepared composite samples due to the instability of silver phosphate under electron beam (see the Supporting Information, Fig. S2).

Our results of Rh. B photodegradation under monochromatic irradiation show that a combination of silver and Ag$_3$PO$_4$ (i.e., Ag/Ag$_3$PO$_4$) significantly enhanced the photocatalytic activity of Ag$_3$PO$_4$. As an example, Fig. 2 compares Rh. B photodegradation under 350 nm on Ag/Ag$_3$PO$_4$-2 with pure Ag$_3$PO$_4$ under same conditions. At 4 min, 72% of Rh. B was degraded on Ag/Ag$_3$PO$_4$-2 (Ag/Ag$_3$PO$_4$ weight ratio being 2.7%) compared with 36.8% on Ag$_3$PO$_4$, unmistakably showing a clear photocatalytic activity enhancement in the presence of metallic silver. Furthermore, the results of Rh. B
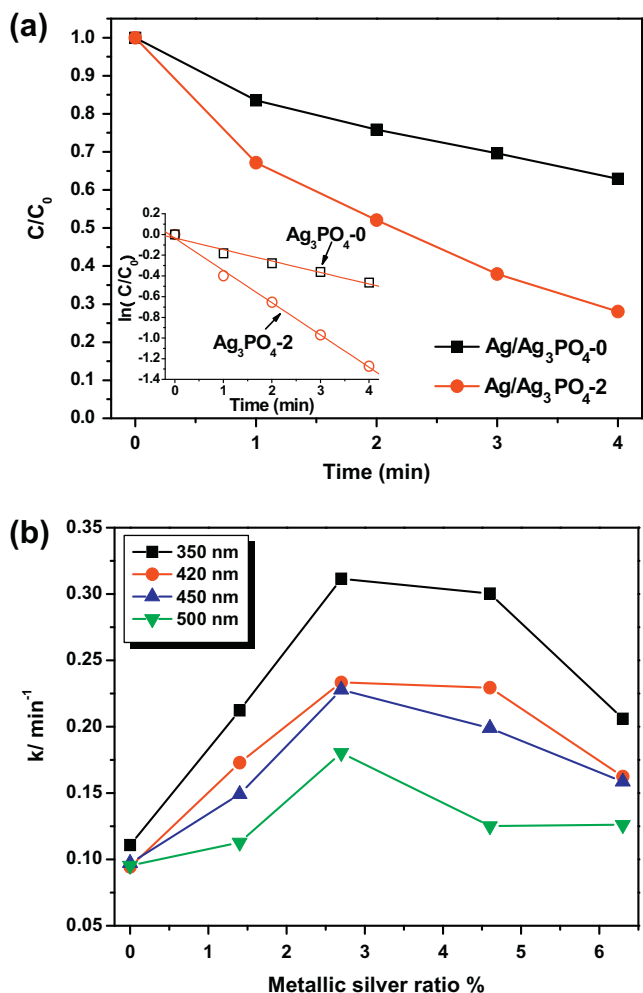
Fig. 2. Concentration variation (C/C_0) of Rh. B over Ag/Ag$_3$PO$_4$–0 and Ag/Ag$_3$PO$_4$–2 under monochromatic lights (350 nm) irradiation (a), and effect of irradiation of different monochromatic lights on pseudo-1st-order kinetic constants of metallic silver coverage amount (b) (dosage = 40 mg/80 mL).

adsorption kinetics and isotherms show that the presence of silver nanoparticles on Ag$_3$PO$_4$ actually decreased its adsorption capacity toward Rh. B (see the Supporting Information, Figs. S3, S4, Table S5, S6), ruling out the possibility of an adsorption contribution to the photocatalytic enhancement in the presence of Ag^0.

The photodegradation kinetics of Rh. B degradation in this study is well fitted with Langmuir–Hinshelwood model [25]. The model fitted value of k obtained for Rh. B degradation on Ag/Ag$_3$PO$_4$–2 and Ag$_3$PO$_4$ was 0.32 min^{-1} and 0.11 min^{-1} under 350 nm irradiation, indicating an almost threefold enhancement in terms of reaction kinetic rate constant.

The Rh. B photodegradation experiments were also conducted with different monochromatic lights (i.e., 420, 450, 500 nm) and with different Ag/Ag$_3$PO$_4$ weight ratios, and corresponding k was calculated and presented in Fig. 2b, which describes the dependence of k on monochromatic wavelengths of incident light and metallic silver ratio %. No Rh. B degradation could be found in the blank experiments without the presence of photocatalysts. It can be clearly noticed from the figure that k, under identical experimental conditions, increased with an increase in metallic silver ratio 0.1 % to 2.7% followed by a decrease at higher values, indicating an optimal level of metallic silver coverage on Ag$_3$PO$_4$ surface for a maximum photocatalytic activity enhancement. Furthermore, the Rh. B degradation on Ag/Ag$_3$PO$_4$ shows an unambiguous depen-

dence on incident light wavelengths where k is decreasing with increasing the incident wavelengths in our case.

In order to quantify photocatalytic activity enhancement by the presence of metallic silver on Ag$_3$PO$_4$, we propose a term: enhancement factor (FE$_{\lambda r}$), which is expressed as follows:

$$FE_{\lambda r} = \frac{k_{\lambda r}}{k_{\lambda 0}} \tag{7}$$

where λ and r denote the wavelength of incident light and metallic silver ratio value, respectively; $k_{\lambda 0}$ and $k_{\lambda r}$ represent k for the photodegradation over pure phase Ag$_3$PO$_4$ and Ag/Ag$_3$PO$_4$ with a metallic silver ratio of r under incident light (λ). The values of FE$_{\lambda r}$ obtained under our experimental conditions are listed in Table 1, which clearly demonstrate that FE$_{\lambda r}$ has interesting and universal features: (1) with all FE$_{\lambda r}$ (from 1.2 to 2.8) being greater than unity, it clearly demonstrates the photoactivity enhancement in all cases in the presence of Ag^0; (2) an optimal Ag^0 level is present at a value where FE$_{\lambda r}$ is the highest for the same λ; (3) FE$_{\lambda r}$ is highly λ dependent, with FE$_{350r}$ > FE$_{420r}$ > FE$_{450r}$ > FE$_{500r}$. It should also be noted that it is not the intention of this manuscript to generalize that FE decreases with increasing λ.

For the first time, our results provide clear evidences that the plasmonic effect of Ag^0 on the photoactivity of Ag$_3$PO$_4$ is Ag^0 weight ratio and incident light wavelength dependent. To ascertain the mechanism behind photodegradation performance enhancement, a physics simulation was conducted. When the Ag$_3$PO$_4$ is illumined by the light, metallic silver nanoparticles are produced on the surface of Ag$_3$PO$_4$. If the number of silver nanoparticles increases, they will cluster with each other. The radius of the Ag$_3$PO$_4$ (with micrometer size) is significantly larger than that of the nanosphere and the incident wavelength. Hence, the nanosphere layer can be approximated as a planar surface. The real part of the refractive index of contaminated water is approximated as n = 1.33, and the imaginary part of refractive index k can be obtained from that of the model compound. The absorption coefficient of the selected model compound is depicted in Fig. 3a. Due to the nonuniform photoreduction in silver on the surface of Ag$_3$PO$_4$, the agglomerated silver particles can form a corrugated metallic layer above Ag$_3$PO$_4$ surface with a fraction of area. SPRs are electromagnetic excitations propagating at the interface between a dielectric and a metal, evanescently confined in the perpendicular direction. Solving Maxwell's equations under the appropriate boundary conditions yields the dispersion relation of surface plasmon polariton (SPP), that is, the frequency-dependent SPP momentum [26,27],
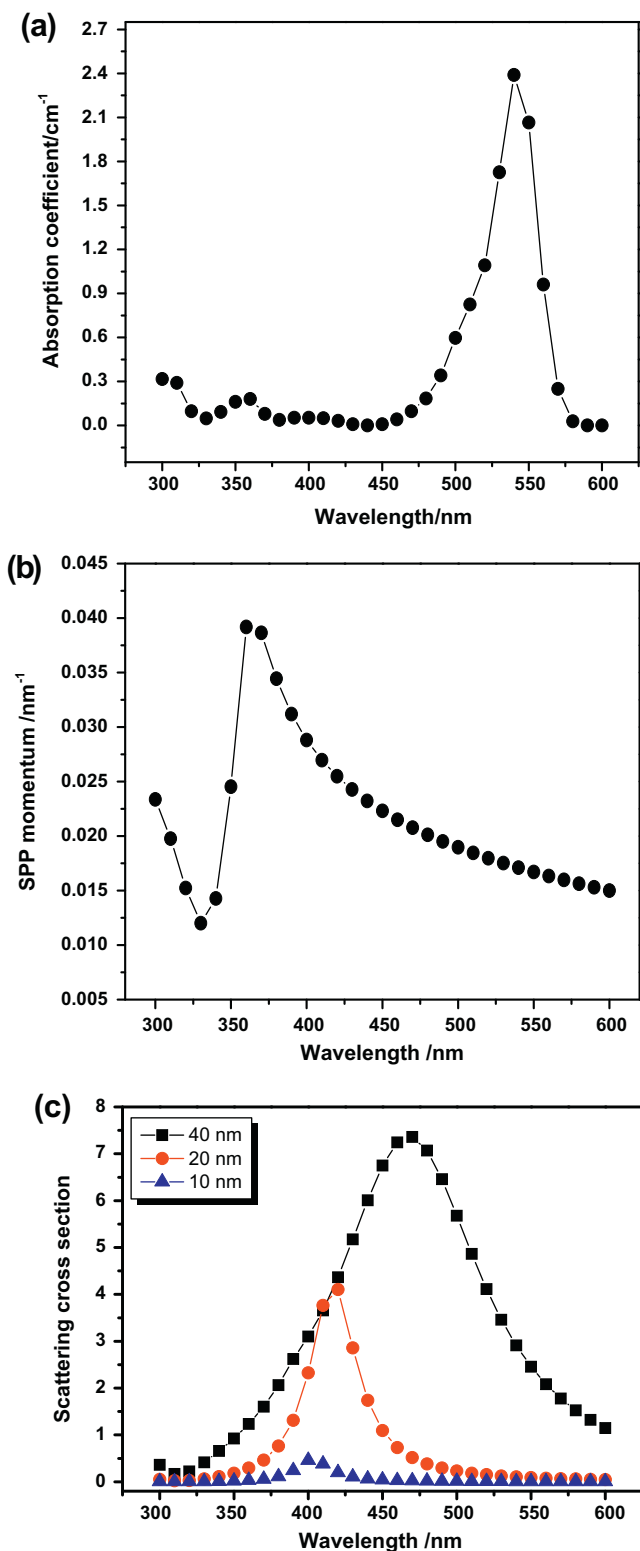
$$k_{sp} = k_0 \sqrt{\frac{\varepsilon_d \varepsilon_m}{\varepsilon_d + \varepsilon_m}} \tag{8}$$

where $k_0 = \frac{2\pi}{\lambda}$ is the wave number of free space, and λ is the wavelength of incident light. The frequency-dependent permittivity of the metal ε_m and the dielectric material ε_d must have opposite signs if SPPs are to be possible at such an interface. The complex permittivity of silver can be expressed by the Brendel–Bormann model [28] and that of Rh. B is taken from [29] ($\varepsilon_{Ag} < 0$ and $\varepsilon_{Rh.B(aq.)} > 0$).

Therefore, SPPs can support at the interface between silver and Rh. B with the momentum as shown in Fig. 3b, the peak of the SPP momentum indicates a surface plasmon resonance having strong

Table 1
Enhancement factors FE$_{\lambda r}$ of series of Ag/Ag$_3$PO$_4$ samples under monochromatic light irradiation using different wavelengths.

	r = 1.4%	r = 2.7%	r = 4.6%	r = 6.3%
λ = 350 nm	1.9	2.8	2.7	1.9
λ = 420 nm	1.8	2.5	2.4	1.7
λ = 450 nm	1.5	2.3	2.0	1.6
λ = 500 nm	1.2	1.9	1.3	1.3

Fig. 3. The absorption coefficient of Rh. B aqueous solution with concentration of 10 μM (a), scattering cross section of an Ag sphere in Rh. B aqueous solution (b) and momentum of surface plasmon polariton traveling between Ag and Rh. B aqueous solution half spaces (c).

The permittivity of silver is larger than zero, and no SPP exists when the incident wavelength becomes smaller than 330 nm. The photoactivity of Ag/Ag_3PO_4 composite is significantly enhanced at the specific wavelength of surface plasmon resonance.

It is worth mentioning that Mie series is employed to compute the scattering cross section of a single silver nanoparticle (assuming the silver particle size of 10 nm, 20 nm and 40 nm) in Rh. B background (as depicted in Fig. 3c), and the associated LSPR could not have a good spectral agreement with the enhancement peak of photoactivity. However, the agglomeration of silver nanoparticles cannot be avoided, and the assumption of corrugated thin metallic layer as well as supported surface plasmon resonance is reasonable. Extensive agglomeration of silver nanoparticles will partially cover the Ag_3PO_4 surface, so that the reaction of Ag_3PO_4 with Rh. B will be gradually inhibited. This is the reason why the adsorption kinetics rate and capacity decreased after the silver particles agglomerate extensively.

4. Conclusions

In summary, this paper reports the photodegradation enhancement on Ag/Ag_3PO_4 composites by plasmonic effect. It was found that both factors such as combined metallic silver amount and the wavelength of incident photons could dramatically influence the photoactivity improvement. The highest photoactivity was obtained under an optimum coverage amount of silver nanoparticles (2.7%) and incident lights having a wavelength of 350 nm. Simulation results suggest that SPR have a good spectral agreement with the enhancement peak of photoactivity rather than LSPR.

Appendix A. Supplementary material

Supplementary data associated with this article can be found, in the online version, at http://dx.doi.org/10.1016/j.jcis.2012.09.086.

References

[1] A. Fujishima, K. Honda, Nature 238 (1972) 37–38.
[2] R. Asahi, T. Morikawa, T. Ohwaki, K. Aoki, Y. Taga, Science 293 (2001) 269–271.
[3] Z. Zou, J. Ye, K. Sayama, H. Arakawa, Nature 414 (2001) 625–627.
[4] A. Kudo, Y. Miseki, Chem. Soc. Rev. 38 (2009) 253–278.
[5] C. Chen, W. Ma, J. Zhao, Chem. Soc. Rev. 39 (2010) 4206–4219.
[6] Z. Yi, J. Ye, N. Kikugawa, T. Kako, S. Ouyang, S. Hilary, H. Yang, J. Cao, W. Luo, Z. Li, Y. Liu, R. Withers, Nat. Mater. 9 (2010) 559–564.
[7] Y. Bi, S. Ouyang, N. Umezawa, J. Cao, J. Ye, J. Am. Chem. Soc. 133 (2011) 6490–6492.
[8] C. Dinh, T. Nguyen, F. Kleitz, T. Do, Chem. Commun. 47 (2011) 7797–7799.
[9] Y.P. Bi, H.Y. Hu, S.X. Ouyang, Z.B. Jiao, G.X. Lu, J.H. Ye, J. Mater. Chem. 22 (2012) 14847–14850.
[10] Y.P. Bi, H.Y. Hu, S.X. Ouyang, Z.B. Jiao, G.X. Lu, J.Y. Cao, J.H. Ye, Chem. Commun. 48 (2012) 3748–3750.
[11] R. Que, Front. Optoelectron. China 4 (2011) 176–180.
[12] Y. Bi, S. Ouyang, J. Cao, J. Ye, Phys. Chem. Chem. Phys. 13 (2011) 10071–10075.
[13] H. Huang, X. Li, Z. Kang, Dalton Trans. 39 (2010) 10593–10597.
[14] P. Wang, B. Huang, X. Qin, X. Zhang, Y. Dai, J. Wei, M. Whangbo, Angew. Chem. Int. Ed. 47 (2008) 7931–7933.
[15] H. Xu, H. Li, J. Xia, S. Yin, Z. Luo, L. Liu, L. Xu, ACS Appl. Mater. Interfaces 3 (2011) 22–29.
[16] A. Baba, P. Taranekar, R. Ramakrishna, W. Knoll, C. Rigoberto, ACS Appl. Mater. Interfaces 2 (2010) 2347–2354.
[17] S. Gao, K. Ueno, H. Misawa, Acc. Chem. Res. 44 (2011) 251–260.

near-field intensity, and the highest SPP momentum of silver nanoparticles, which can be reached under incident photons with wavelength of $\sim$ 359 nm, which is well coincident with the experimental results and calculated enhancement factor ($FE_{\lambda r}$).

[18] W. Sha, W. Choy, W. Chew, Opt. Express 18 (2010) 5993–6007.
[19] Q. Yu, R. Zhang, S. Deng, J. Huang, G. Yu, Water Res. 43 (2009) 1150–1158.
[20] I. Langmuir, J. Am. Chem. Soc. 38 (1916) 2221–2295.
[21] H. Freundlich, Z. Phys. Chem. 57 (1906) 385–470.
[22] C.F. Bohren, D.R. Huffman, Absorption and Scattering of Light by Small Particles, Wiley Interscience, 1998.
[23] W.C. Chew, Waves and Fields in Inhomogenous Media, Wiley IEEE Press, 1999.
[24] L. Tsang, J.A. Kong, K.H. Ding, Scattering of Electromagnetic Waves: Theories and Applications, Wiley, 2000.
[25] K. Kumar, K. Porkodi, F. Rocha, Catal. Commun. 9 (2008) 82–84.
[26] W. Barnes, A. Dereux, T. Ebbesen, Nature 424 (2003) 824–830.
[27] S.A. Maier, Plasmonics: Fundamentals and Applications, Springer, 2007.
[28] A. Rakic, A. Rakic, B. Djurisic, M. Majewski, Appl. Opt. 37 (1998) 5271–5283.
[29] B. Rossi, H. Byrne, W. Blau, Appl. Phys. Lett. 58 (1991) 1712–1714.